



UNIVERSITY OF LEEDS

This is a repository copy of *Indolin-2-one derivatives as selective Aurora B kinase inhibitors targeting breast cancer*.

White Rose Research Online URL for this paper:

<https://eprints.whiterose.ac.uk/180154/>

Version: Accepted Version

Article:

Dokla, EME, Abdel-Aziz, AK, Milik, SN et al. (5 more authors) (2021) Indolin-2-one derivatives as selective Aurora B kinase inhibitors targeting breast cancer. *Bioorganic Chemistry*, 117. 105451. 105451-. ISSN 0045-2068

<https://doi.org/10.1016/j.bioorg.2021.105451>

© 2021 Elsevier Inc. All rights reserved. This manuscript version is made available under the CC-BY-NC-ND 4.0 license <http://creativecommons.org/licenses/by-nc-nd/4.0/>.

Reuse

This article is distributed under the terms of the Creative Commons Attribution-NonCommercial-NoDerivs (CC BY-NC-ND) licence. This licence only allows you to download this work and share it with others as long as you credit the authors, but you can't change the article in any way or use it commercially. More information and the full terms of the licence here: <https://creativecommons.org/licenses/>

Takedown

If you consider content in White Rose Research Online to be in breach of UK law, please notify us by emailing eprints@whiterose.ac.uk including the URL of the record and the reason for the withdrawal request.



eprints@whiterose.ac.uk
<https://eprints.whiterose.ac.uk/>

Indolin-2-one Derivatives as Selective Aurora B Kinase Inhibitors

Targeting Breast Cancer

Eman M. E. Dokla^{a,*†}, Amal Kamal Abdel-Aziz^{b,c†}, Sandra N. Milik^{a,d,†}, Amr H. Mahmoud^e, Mona Kamal Saadeldin^{c,f}, Martin J. McPhillie^d, Saverio Minucci^{c,f,¥,*}, Khaled A. M. Abouzid^{a,g,¥}

^a *Pharmaceutical Chemistry Department, Faculty of Pharmacy, Ain Shams University, Abbassia, Cairo 11566, Egypt*

^b *Department of Pharmacology and Toxicology, Faculty of Pharmacy, Ain Shams University, Abbassia, Cairo, 11566, Egypt*

^c *Department of Experimental Oncology, IEO, European Institute of Oncology IRCCS, Via Adamello 16, 20139, Milan, Italy*

^d *School of Chemistry, University of Leeds, Leeds LS2 9JT, United Kingdom*

^e *Department of Pharmaceutical Sciences, University of Basel, Klingelbergstrasse 50, 4056, Basel, Switzerland*

^f *Department of Biosciences, University of Milan, Milan, 20100, Italy*

^g *Department of Organic and Medicinal Chemistry, Faculty of Pharmacy, University of Sadat City, Sadat City, 32897, Egypt*

*Corresponding author.

E-mail address: emanelawady@pharma.asu.edu.eg (E.M.E. Dokla); Saverio.Minucci@ieo.it (S. Minucci)

†These authors have equal contributions.

¥ These authors are co-senior authors

Abstract

Aurora B is a pivotal cell cycle regulator where errors in its function results in polyploidy, genetic instability, and tumorigenesis. It is overexpressed in many cancers, consequently, targeting Aurora B with small molecule inhibitors constitutes a promising approach for anticancer therapy. Guided by structure-based design and molecular hybridization approach we developed a series of fifteen indolin-2-one derivatives based on a previously reported indolin-2-one-based multikinase inhibitor (**1**). Seven derivatives, **5g**, **6a**, **6c-e**, **7**, and **8a** showed preferential antiproliferative activity in NCI-60 cell line screening and out of these, carbamate **6e** and cyclopropylurea **8a** derivatives showed optimum activity against Aurora B ($IC_{50} = 16.2$ and 10.5 nM respectively) and MDA-MB-468 cells ($IC_{50} = 32.6 \pm 9.9$ and 29.1 ± 7.3 nM respectively). Furthermore, **6e** and **8a** impaired the clonogenic potential of MDA-MB-468 cells. Mechanistic investigations indicated that **6e** and **8a** induced G2/M cell cycle arrest, apoptosis, and necrosis of MDA-MB-468 cells and western blot analysis of **8a** effect on MDA-MB-468 cells revealed **8a**'s ability to reduce Aurora B and its downstream target, Histone H3 phosphorylation. **6e** and **8a** displayed better safety profiles than multikinase inhibitors such as sunitinib, showing no cytotoxic effects on normal rat cardiomyoblasts and murine hepatocytes. Finally, **8a** demonstrated a more selective profile than **1** when screened against ten related kinases. Based on these findings, **8a** represents a promising candidate for further development to target breast cancer via Aurora B selective inhibition.

Keywords

Aurora B; kinase inhibitor; breast cancer; indolin-2-one; molecular hybridization

1. Introduction

Aurora B is a serine/threonine kinase that plays a crucial role in controlling the cell cycle, particularly the mitotic and cytokinesis phase [1]. It is responsible for proper chromosome segregation and cytokinesis [2] serving as a mitotic checkpoint, where errors in its function results in increased aneuploidy, genetic instability, and tumorigenesis [3]. Aurora B was reported to be overexpressed in numerous cancers including breast, ovarian, colorectal, and lung cancers [4] and evidence showed that inhibition of Aurora B in tumors led to dysregulation of mitotic checkpoint which resulted in polyploidy and subsequent cell death [5]. Therefore, Aurora B represents a promising target for anticancer therapy.

Several pan-Aurora and selective Aurora B kinase inhibitors were developed over the last two decades and many of these are currently undergoing clinical trials (phase I or II) [6] but to date, no Aurora B kinase inhibitor has been approved yet [7–10]. Pan-Aurora kinase inhibitors comprise VX-680 [11], AT9283 [12], and ZM447439 [13], while specific Aurora B kinase inhibitors include the ATP competitive inhibitors, hesperadin [14] and barasertib [15], and the recently reported non-ATP competitive inhibitor SP-96 [16] (**Figure 1**). Both Aurora B kinase inhibition and combination with conventional chemotherapy showed good efficacy in preclinical models [17], and since many of these inhibitors showed off-target inhibition, more selective Aurora B kinase inhibitors are in demand [9].

Owing to sunitinib potency as a multikinase inhibitor [18,19], a multitude of kinase inhibitors were developed based on the indolin-2-one moiety [20,21], many of these were type II kinase inhibitors designed to show less promiscuity by attaining selectivity against specific kinase targets [22–24]. Aurora B inhibitors based on the indolin-2-one scaffold comprises the previously mentioned hesperadin, SU6668 [25], and BI-847325 [26] (**Figure 1**).

Considering the efficacy of the pyrrole indolin-2-one unit as a hinge binder [27–29], we utilized the ChEMBL database to identify pyrrole indolinone-based kinase inhibitors with reported activity against Aurora B [30]. A previously reported Chk1 kinase inhibitor, (*Z*)-3-((1*H*-pyrrol-2-yl)methylene)-6-(4-hydroxyphenyl)indolin-2-one (**1**) [31] (**Figure 1**) showing potent activity against Aurora B kinase ($K_i = 19.95$ nM) was identified and selected as a lead compound.

Our aim was to optimize this multikinase inhibitor into a more potent Aurora B inhibitor with enhanced kinase selectivity profile and test its anti-tumor properties in breast cancer cells. Guided by structure-based design and molecular hybridization approach, we developed a series of indolin-2-one derivatives and identified **8a** as a potent and selective Aurora B inhibitor showing preferential antiproliferative profile with nanomolar activity against MDA-MB-468 breast cancer cell line and minimal cytotoxicity against normal cell lines.

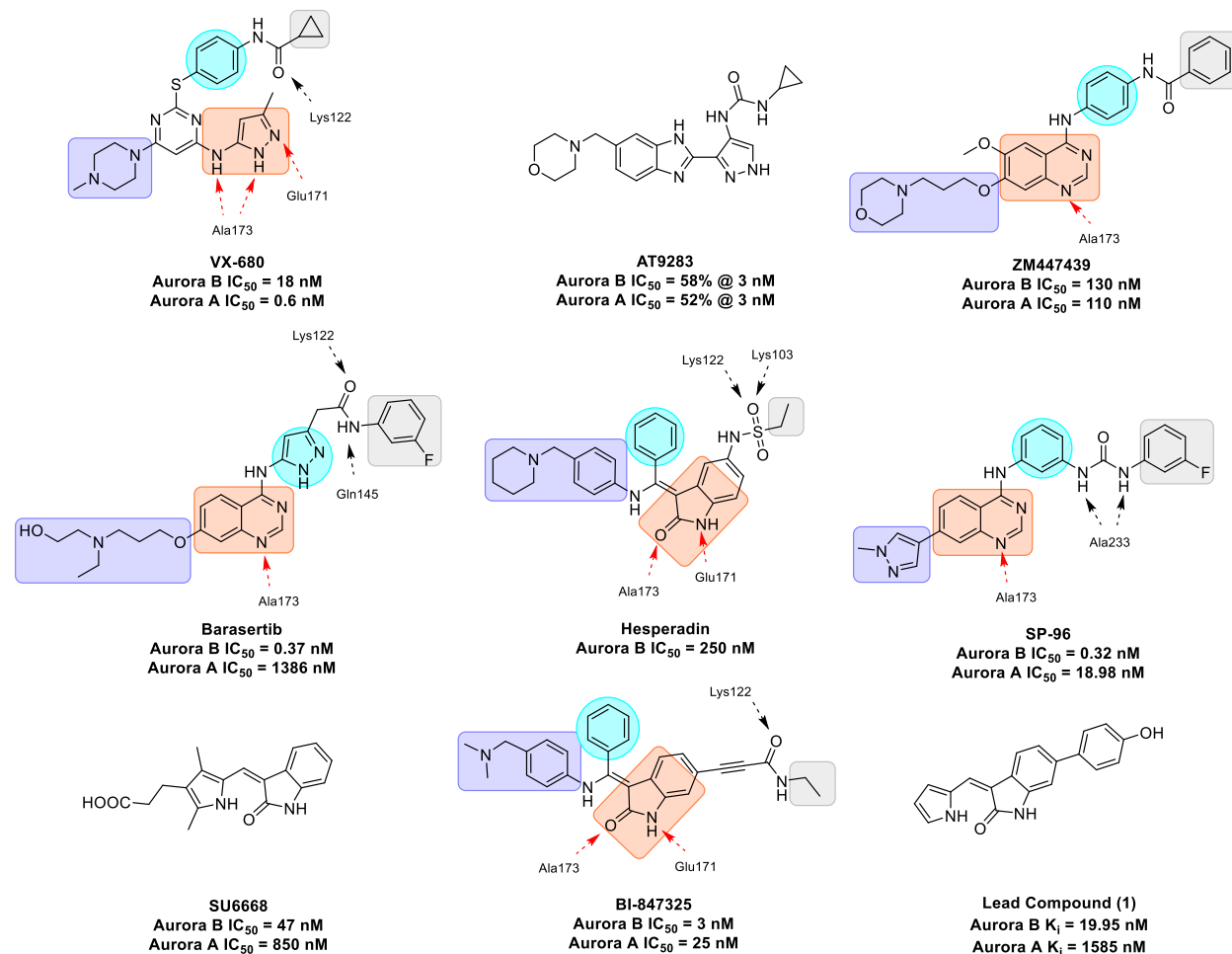


Figure 1. Chemical structures and predicted binding modes of reported Aurora B kinase inhibitors. Binding modes of **VX-680**, **ZM447439**, **barasertib**, **hesperadin**, **BI-847325** were predicted in reference to their x-ray crystal structures with Aurora B kinase (PDB codes: 4AF3, 2VRX, 4C2V, 2BFY, and 5EYK respectively), while **SP-96** binding mode was predicted based on its molecular docking pose [16]. Different binding regions are displayed as follows: adenine pocket (orange), hydrophobic region (cyan), solvent accessible region (purple), and allosteric pocket (grey). Broken arrows represents hydrogen bonds with respective amino acids. No crystal structures or docking studies were reported for **AT9283**, **SU6668**, or **1** with Aurora B.

2. Results and Discussion

2.1. Design Strategy

Public databases for chemical compounds and their biological data provide an ever-expanding source for data mining for the purpose of drug discovery [32–35]. Of these, the ChEMBL database represents the main source for small molecules' bioactivity data [36]. Guided by our interest in developing selective Aurora B kinase inhibitors and the frequent reports of the indolin-2-one scaffold as an efficient hinge binder, we searched the ChEMBL database for small molecules containing pyrrole indolin-2-one moiety with reported Aurora B kinase inhibitory activity. We identified a pyrrole indolinone-based Chk-1 kinase inhibitor (**1**) as our lead with reported nanomolar activity against Aurora B kinase ($K_i = 19.95$ nM) and more than a dozen other kinases including, Abl1, ALK, JAK2, JAK3, VEGFR2, PDGFR β , RET, LRRK2 and others [36]. We started by revalidating the lead compound (**1**) activity using SelectScreen kinase profiling service where it showed an IC_{50} of 84.4 nM against Aurora B kinase enzyme.

In order to optimize compound **1**, we needed to understand how it binds to Aurora B kinase enzyme. Compound **1** was docked into the ATP binding site of Aurora B kinase using CDOCKER module of Discovery Studio[®] 2.5 software and analyzed the resulting binding mode. As presented in **Figure 2**, compound **1** binds in a similar mode to the reported Aurora B inhibitors, where the indolin-2-one moiety fits in the hinge region and forms two hydrogen bonds with Ala173 and Glu171, additionally the pyrrole nitrogen forms a hydrogen bond with Ala173. The *p*-hydroxyphenyl moiety at 6-position extends into the hydrophobic pocket and forms a hydrogen bond between the hydroxyl group and Gln145. An unoccupied allosteric pocket (the enzyme is in “DFG-out” conformation) is revealed which can be exploited to design more selective Aurora B kinase inhibitors. We herein report our efforts to optimize the lead compound (**1**) by varying the substituents at the indolin-2-one 6-phenyl moiety and further extending these substituents into the allosteric pocket.

Molecular hybridization is an established strategy for drug discovery that combine two or more fragments from different molecules to produce new hybrid compounds designed for various goals. These might include, increased potency, improved selectivity, better metabolic

stability, or even aiming at a different target [37,38]. Based on our understanding of the binding modes of different reported Aurora B kinase inhibitors, we incorporated several moieties from these inhibitors into the 6-phenyl group of our designed compounds to target the allosteric pocket, including cyclopropylamide (VX-680), cyclopropylurea (AT9283), and benzamide (ZM447439).

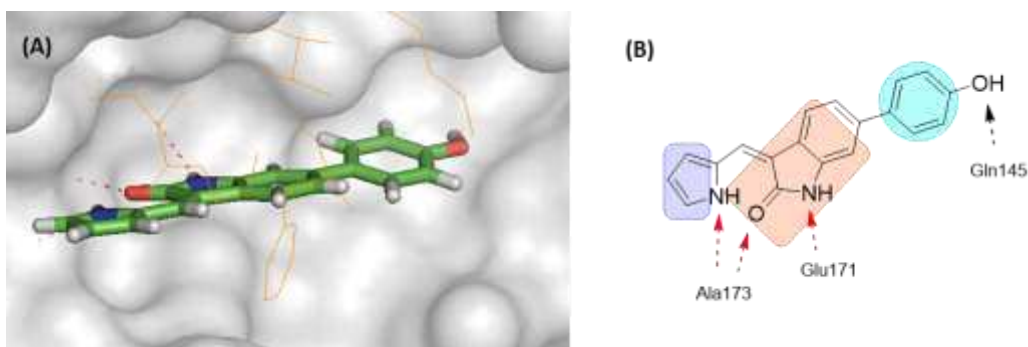
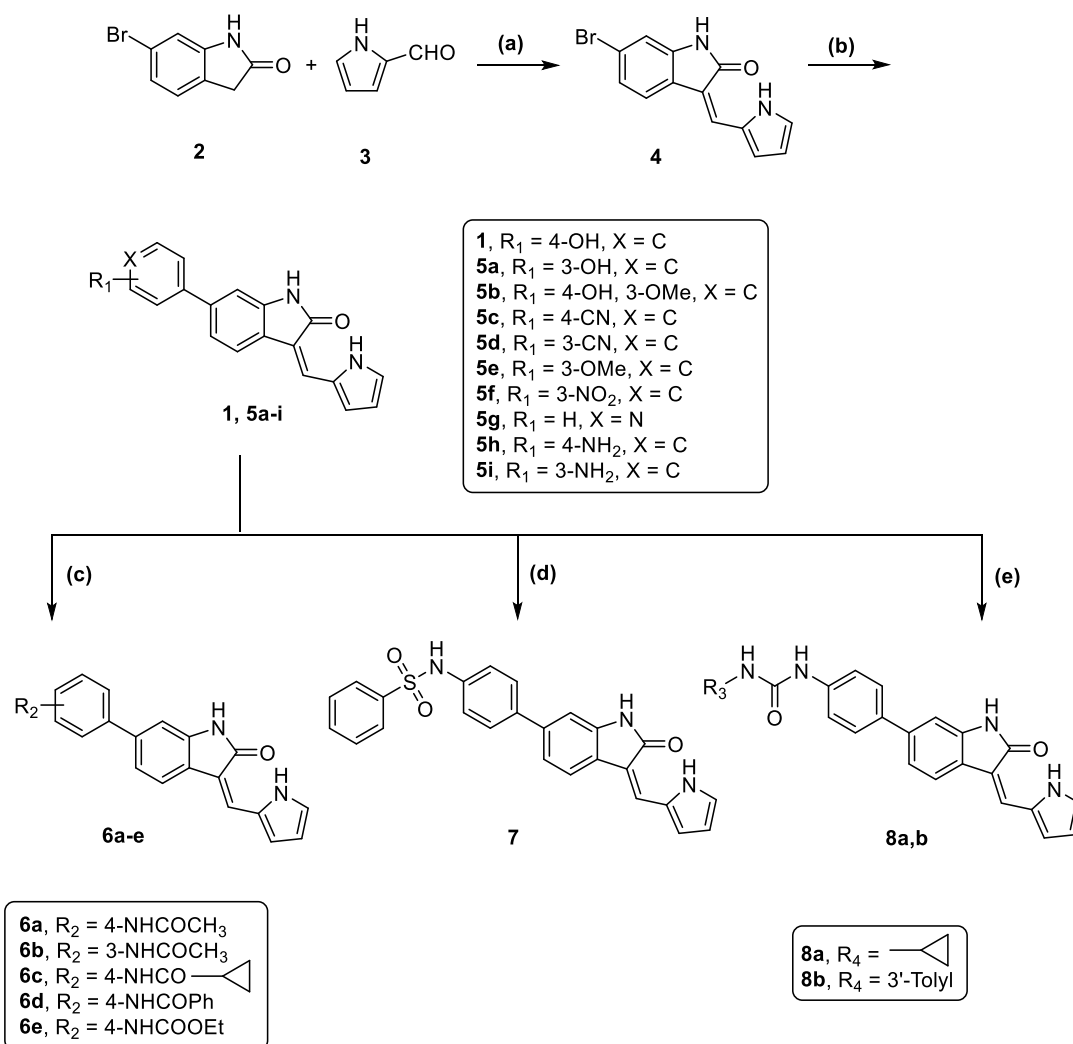


Figure 2. (A) Docking of lead compound (**1**) into the ATP binding site of Aurora B kinase enzyme (PDB code: 4C2V) revealed an unoccupied allosteric pocket. The figure was visualized using PyMOL. (B) Predicted binding mode of compound (**1**) based on its molecular docking pose (refer to **Figure 1** for different binding region interpretation).

2.2. Chemistry

The desired indolin-2-one derivatives were synthesized along their lead compound (**1**) according to the previously reported procedures [39–43] as depicted in **Scheme 1**. Knoevenagel condensation of 6-bromoindolin-2-one (**2**) with 1*H*-pyrrole-2-carboxaldehyde (**3**) in toluene using catalytic amount of piperidine and acetic acid yielded the desired (*Z*)-3-((1*H*-pyrrol-2-yl)methylene)-6-bromoindolin-2-one (**4**) in very good yield. Suzuki coupling of bromo derivative (**4**) with the appropriate boronic acid using palladium tetrakis and potassium carbonate in dioxane and water yielded the desired products (**1**, **5a-i**) in poor to very good yields. Amine derivatives (**5h**, **5i**) were further functionalized as amides or carbamate using the appropriate acid chloride or ethyl chloroformate in pyridine to give the desired products (**6a-e**) in fair to good yields. The amine derivative (**5h**) was reacted with benzenesulfonyl chloride in pyridine to furnish the desired sulfonamide derivative (**7**) in fair yield. Urea derivatives (**8a,b**) were synthesized on two steps by first reacting the amine derivative (**5h**) with triphosgene in THF, then the formed isocyanate was reacted with the appropriate amine using DIPEA in THF to give the desired urea derivatives (**8a,b**) in fair yields.



Scheme 1. Reagents and conditions: **(a)** Toluene, AcOH, piperidine, 80°C, 2 h, 82% yield; **(b)** Aryl boronic acid, Pd tetrakis, K₂CO₃, dioxane, H₂O, reflux, 6 h, 15-81% yield; **(c)** **5h** or **5i**, RCOCl, pyridine, rt, 4 h, 55-73% yield; **(d)** **5h**, benzenesulfonyl chloride, pyridine, rt, 24 h, 57% yield; **(e)** **(1)** **5h**, triphosgene, dry THF, reflux, 2 h, **(2)** Amine, DIPEA, THF, reflux, 24 h, 44-61% yield.

2.3. Biological evaluation

2.3.1. *In vitro* Aurora B kinase assay

The synthesized indolin-2-one derivatives were initially evaluated in a single dose assay at 100 nM for their inhibitory activity against Aurora B kinase enzyme (**Table 1**). Only 3-hydroxy (**5a**), amide (**6a-d**), carbamate (**6e**), and urea (**8a,b**) derivatives showed inhibitory activity $\geq 90\%$ at 100 nM and were further evaluated for their IC₅₀ along with the lead compound (**1**). The 3-hydroxy (**5a**) and 3-acetamido (**6b**) derivatives showed single digit nanomolar activity against

Aurora B enzyme (5.8 and 7.8 nM respectively), while the remaining six derivatives (**6a,c-e** and **8a,b**) showed activity ranging from 10-20 nM (**Table 1**). As evident by these results, substitution of the 6-phenyl moiety with bulkier substituent capable of forming hydrogen bonds with the amino acid residues at the allosteric pocket mostly yielded more potent derivatives than the lead compound (**1**) ($IC_{50} = 84.4$ nM).

Table 1. *In vitro* Aurora B kinase inhibition and antiproliferative activities of the indolin-2-one derivatives **1**, **5a-g**, **6a-e**, **7**, and **8a,b**.

Compounds	AURKB ^a Inhibition		MDA-MB-468 IC ₅₀ ^b (nM)
	at 100 nM (%)	IC ₅₀ (nM)	
1	--	84.4	21.0 ± 2.9
5a	93	5.8	--
5b	77	--	--
5c	42	--	--
5d	44	--	--
5e	53	--	--
5f	53	--	--
5g	77	--	--
6a	91	12.5	84.5 ± 11.4
6b	97	7.8	--
6c	97	15.7	75.1 ± 16.9
6d	94	17.6	342.6 ± 90.5
6e	95	16.2	32.6 ± 9.9
7	66	--	--
8a	102	10.5	29.1 ± 7.3
8b	90	19.4	--
Staurosporine	--	5.04	--
Sunitinib malate	--	--	12574 ± 3592.6

^aThe Aurora B kinase inhibition assay was provided by ThermoFisher Scientific. All data were obtained by double testing and expressed as mean values.

^bMedian inhibitory concentration (IC_{50}) values are expressed as mean±SD and were based on the data obtained from triplicates of at least two independent experiments.

2.3.2. *In vitro* antiproliferative screening

One of our design goals was to develop more selective Aurora B kinase inhibitors than the starting lead compound (**1**). Based on the premise that multikinase inhibitors tend to inhibit various cancer cell lines non-selectively [44,45], we elected to use the NCI-60 cell line panel as a rough estimate for our compounds' selectivity. One-dose screening at 10 μ M of our compounds (**Supplementary data, S2-S23**) showed that compounds **1**, **5a-f**, **6b**, **8b** manifested non-selective antiproliferative activity, where they inhibited many to almost all of the screened NCI-60 cell lines. Compounds **5g**, **6a**, **6c-e**, **7**, **8a** showed a much selective antiproliferative profile, where they inhibited a limited number of the NCI-60 cell line panel including, leukemia SR, colon cancer KM-12, and breast cancer MCF-7, T-47D, and MDA-MB-468 cell lines suggesting a more selective mode of action.

MDA-MB-468 is an aneuploid human basal-like triple negative breast cancer cell line that overexpresses Aurora B kinase enzyme compared to other breast cancer cell lines [46]. Indeed, MDA-MB-468 cells have been reported to be more vulnerable to the anticancer activities of Aurora B kinase inhibitors [46,47]. To this end, we decided to evaluate the potential anticancer activity of the synthesized compounds on MDA-MB-468 cells using the CellTiter-Glo[®] Luminescent Cell Viability Assay. We chose to focus on compounds **6a**, **6c-e**, **8a** in light of their potent activity against Aurora B kinase enzyme and their discriminative profile against the NCI-60 cell lines. Consistent with the results of Aurora B kinase enzyme inhibition assay, carbamate (**6e**) and cyclopropylurea (**8a**) derivatives demonstrated the most potent anticancer activities against MDA-MB-468 with IC_{50} of 32.6 ± 9.9 and 29.1 ± 7.3 nM respectively (**Table 1**). Similarly, in line with the NCI-60 cell lines screening results demonstrating non-selective potent anticancer activity against almost all cancer cells, compound **1** showed an IC_{50} of 21.0 ± 2.9 nM on MDA-MB-468 cells. In contrast, sunitinib demonstrated modest anticancer activity on MDA-MB-468 cells with an IC_{50} of 12574 ± 3592.6 nM as previously reported [48].

Aurora kinase B inhibitors have been reported to decrease the colony forming potential of diverse types of cancer [47–50]. To determine whether compounds **6e** and **8a** could affect the clonogenic potential of breast cancer cells, MDA-MB-468 cells seeded at a low density were

treated with vehicle, **6e** or **8a**. After 14 days, colonies were stained with crystal violet and counted. Indeed, compounds **6e** and **8a** significantly impaired the ability of MDA-MB-468 cells to form colonies (**Figure 3**). Altogether, these data demonstrate the potent *in vitro* anticancer activity of compounds **6e** and **8a** on triple negative breast cancer (MDA-MB-468) cells.

Figure.3

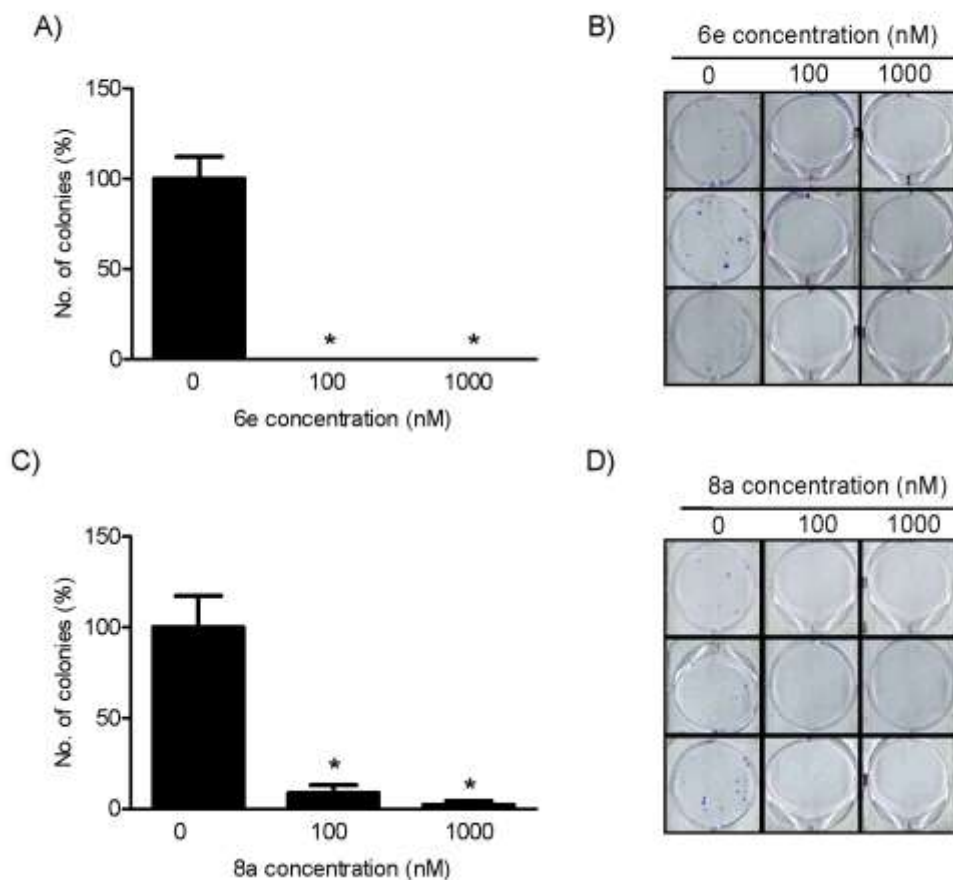


Figure 3. Compounds 6e and 8a evidently impeded the colony forming potential of MDA-MB-468 breast cancer cells. (A), (C) Percent of number of colonies of MDA-MB-468 cells 14 days following their treatment with the indicated concentrations of compounds **6e** and **8a**, respectively. *: Statistical significance as compared to vehicle-treated group assessed using One way analysis of variance (ANOVA) followed by Dunnett test for post-hoc analysis. **(B), (D)** Representative images of fixed and crystal violet stained colonies of MDA-MB-468 cells 14 days following their treatment with the indicated concentrations of compounds **6e** and **8a**, respectively.

2.3.3. Cell cycle analysis of compounds 6a and 8a

Aurora B kinase is the catalytic component of the chromosomal passenger complex which orchestrates proper chromatid segregation at mitosis and cytokinesis [51]. Pharmacological as

well as genetic interference with Aurora B result in premature mitotic exit and cell cycle arrest in the G2/M phase followed by apoptotic cell death [52]. Thereof, the DNA content of MDA-MB-468 cells treated with vehicle, compounds **6e** or **8a** were assessed using flow cytometry. Indeed, compounds **6e** and **8a** increased the percent of 4N MDA-MB-468 cells as evidenced by prominent arrest in the G2/M phase (**Figure 4**).

Figure.4

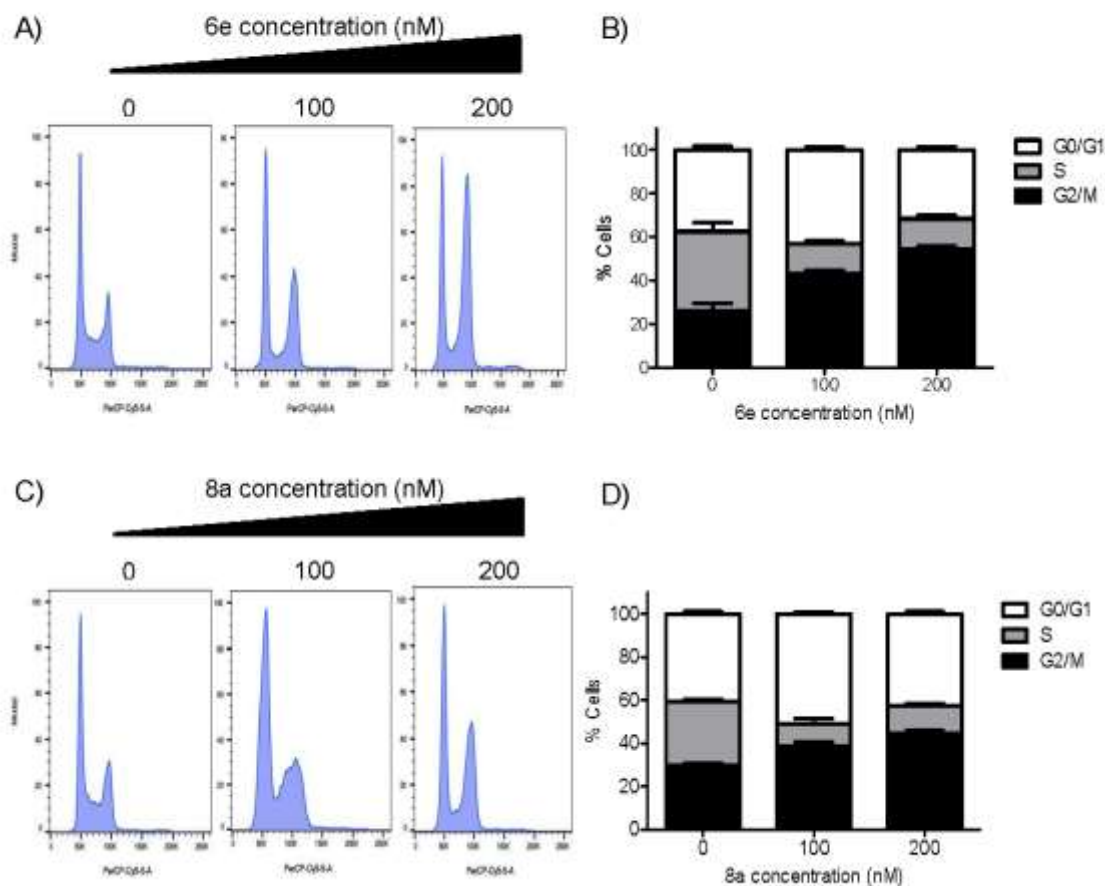


Figure 4. Compounds 6e and 8a trigger G2/M cell cycle arrest in MDA-MB-468 breast cancer cells. (A), (C) Representative flow cytometric histograms depicting the cell cycle distribution of MDA-MB-468 cells 24 h following their treatment with either vehicle or the indicated concentrations of compounds **6e** and **8a**, respectively. **(B), (D)** Percentages of MDA-MB-468 cells in G0/G1, S and G2/M phase 24 h following their treatment with the indicated concentrations of compounds **6e** and **8a**, respectively.

Next, to evaluate whether compounds **6e** and **8a** could trigger cell death of MDA-MB-468 cells, we exploited propidium iodide (PI), a fluorescent DNA-binding dye, which preferentially

penetrates the cell membranes of apoptotic and necrotic cells. FACS analysis and morphological examination revealed that compounds **6e** and **8a** significantly triggered apoptotic and necrotic death of MDA-MB-468 cells (**Figure 5**). Collectively, these findings indicated that compounds **6e** and **8a** induced G2/M cell cycle arrest followed by apoptotic and necrotic cell death of MDA-MB-468 cells.

Figure.5

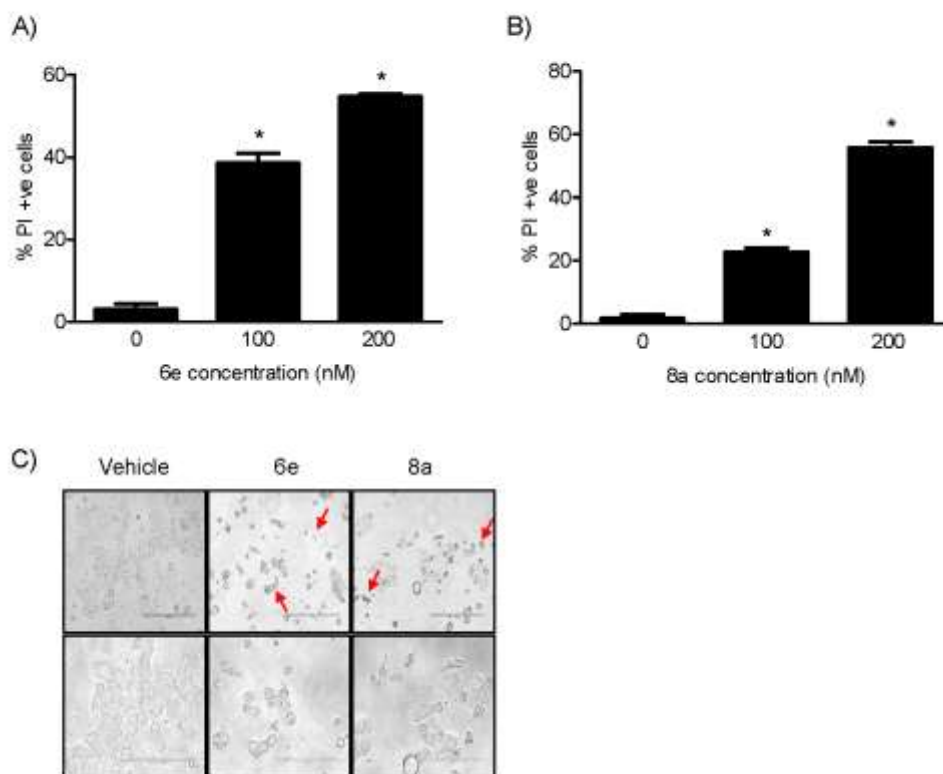


Figure 5. Compounds 6e and 8a induce apoptotic and necrotic cell death of MDA-MB-468 breast cancer cells. (A), (B) Percent of propidium iodide (PI) positive MDA-MB-468 cells following their treatment with the indicated concentrations of compound **6e** and **8a**, respectively for 96 h assessed using flow cytometry. *: Statistical significance as compared to vehicle-treated group assessed using One way analysis of variance (ANOVA) followed by Dunnett test for post-hoc test. **(C)** Phase contrast images of MDA-MB-468 cells following their treatment with vehicle, compound **6e** (100 nM) and **8a** (100 nM) for 96 h. Upper (20x) and lower (40x) panels depicting apoptotic and necrotic cells (red arrows).

2.3.4. Western blot analysis of the effect of compound 8a on MDA-MB-468 cells

Aurora B phosphorylation at Thr-232 is indispensable for its kinase activity and function [53]. Aurora B directly phosphorylates Histone H3 at Serine 10 which plays a fundamental role in

mitotic chromatin condensation [54,55]. Indeed, immunoblot analysis revealed that compound **8a** evidently abrogated the activity of Aurora B in MDA-MB-468 cells as indicated by reduced phosphorylation of Aurora B at Thr232 and its downstream target, Histone H3 at Serine 10 (**Figure 6**).

Figure.6

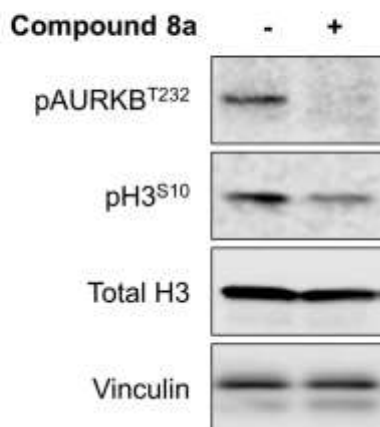


Figure 6. Immunoblot analysis of AURKB and histone H3 in MDA-MB-468 cell lysates 72 h following their treatment with either vehicle or compound **8a** (100 nM). Vinculin was used as a loading control.

2.3.5. Cytotoxic activity of compounds **6e** and **8a** against normal cells

Kinase inhibitors have revolutionized the treatment of patients with diverse types of cancer. However, dose-limiting toxicities and subsequent therapy discontinuation have been reported [56–59]. Cardiotoxicity and hepatotoxicity are among the toxicities associated with kinase inhibitors including sunitinib [56–58]. Thus, we sought to investigate the potential cytotoxic effect of compounds **6e** and **8a** on normal rat cardiomyoblast (H9c2) and murine hepatocyte (BNL) cells. Anticancer concentrations of compounds **6e** and **8a** did not elicit deleterious cytotoxic effects on H9c2 and BNL cells (**Figure 7**). Notably, compounds **6e** and **8a** displayed better safety profiles in terms of both cardio- as well as hepatotoxicities as compared to sunitinib.

[31,36], compound **8a** showed negligible inhibition against Abl1, ALK, Chk1, JAK2, JAK3, and LRRK2 kinases. Furthermore, **8a** showed less than 55% inhibition against VEGFR2, PDGFR β , and RET kinase enzymes exhibiting a more selective profile than its parent compound **1**. Moreover, compound **8a** showed less than 80% inhibition at 1 μ M of the closely related Aurora A kinase indicating a preferential activity for Aurora B over its cognate partner Aurora A.

Table 2. *In vitro* kinase inhibition profile of **8a**.

Kinase	% Inhibition ^a at 1 μ M
ABL1	13
ALK	9
AURKA	74
Chk1	0
JAK2	-1
JAK3	2
VEGFR2	53
PDGFRB	54
RET	50
LRRK2	3

^aThe kinase inhibition assays were provided by ThermoFisher Scientific. All data were obtained by double testing.

2.4. Molecular modeling studies

Docking of the target compounds (**Scheme I**) into the ATP binding site of Aurora B kinase enzyme (PDB:4C2V) using CDOCKER protocol of Discovery Studio[®] 2.5 software revealed a similar binding mode to the crystallized ligand (i.e. barasertib) and the lead compound (**1**) (**Supplementary data, Figure S1**). The docking binding scores for the best poses were calculated using -CDOCKER_INTERACTION_ENERGY (**Supplementary data, Table S1**). Compared to the lead compound's (**1**) - CDOCKER_INTERACTION_ENERGY (43.627 Kcal/mol), compounds **5a**, **5c**, **5d**, **5e**, and **5f** showed lower or similar interaction energy, and all of these compounds except for **5a** showed lower activity when screened against Aurora B kinase enzyme at 1 μ M concentration. Compounds **5b**, **6a-e**, **7**, and **8a,b** showed higher interaction energy compared to **1** and these

compounds showed better activity than **1** when tested against Aurora B kinase enzyme except for compounds **5b** and **7**, which showed less than 80% inhibition at 1 μ M concentration.

Analysis of the best docked pose of **8a** into the ATP binding site of Aurora B kinase enzyme revealed an optimum binding pose and interactions (**Figure 8**). Firstly, the indolin-2-one carbonyl group maintained the essential hydrogen bond with Ala173 at the hinge region and additional hydrogen bonds were evident between the indolin-2-one NH group and Glu 171, and between the pyrrole NH and Ala173. Additionally, the urea moiety was involved in three hydrogen bonds at the allosteric channel with Lys122 and Glu141. Finally, the cyclopropyl fits into a hydrophobic pocket formed of Leu124, Val134, and Leu138.

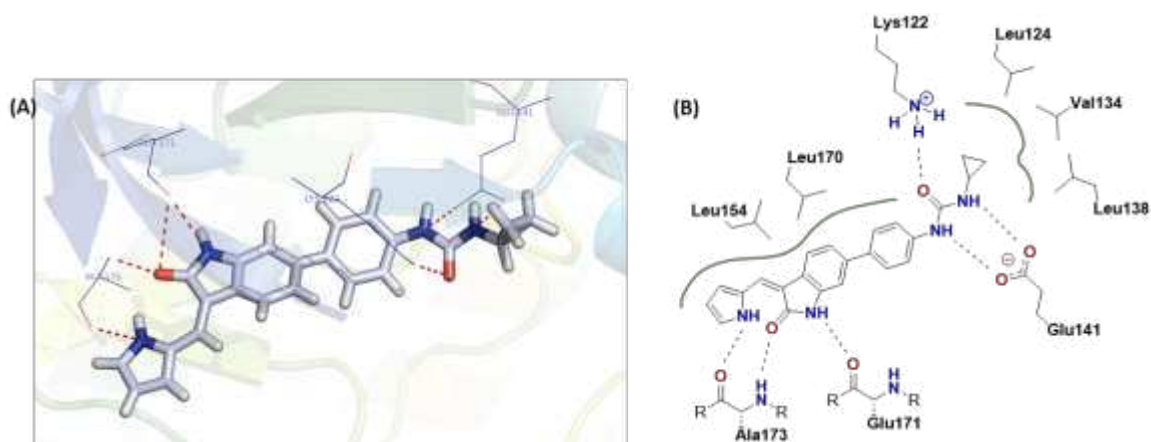


Figure 8. Docking of 8a into the ATP binding site of Aurora B kinase enzyme (PDB code: 4C2V). (A) 3D binding pose of **8a** derivative. **8a** is represented as sticks, interacting amino acids are represented as lines, and hydrogen bonds are depicted in red dotted lines. The figure was visualized using PyMOL. (B) 2D interaction diagram of **8a** displaying the key amino acids involved in this interaction.

3. Conclusion

In this study we report the development of a series of indolin-2-one derivatives as potential Aurora B kinase inhibitors targeting breast cancer via structural optimization of a multikinase inhibitor **1**. Cyclopropylurea derivative (**8a**) showed optimum inhibitory activity against Aurora B kinase and MDA-MB-468 cells, and mechanistic studies indicated that **8a** induced G2/M cell cycle arrest followed by apoptotic and necrotic cell death of MDA-MBA-468 cells. Furthermore, western blot analysis confirmed that **8a** exerted its action by reducing phosphorylation of Aurora B and its downstream target, Histone H3. Regarding **8a** selectivity,

both NCI-60 cell line screening and kinase profiling indicated a more preferential antiproliferative activity and a less promiscuous kinase profile than its lead compound **1**. Moreover, **8a** showed no cytotoxic effects on H9c2 and BNL cells at anticancer concentrations and displayed a better safety profile as compared to sunitinib. Accordingly, compound **8a** represents a promising candidate for further development as targeted therapy for breast cancer via selective Aurora B kinase inhibition.

4. Experimental

4.1. Chemistry

Chemicals and solvents were purchased from Sigma-Aldrich (Germany) and Alfa Aesar (Germany) and were used as such without further purification. Reactions were followed using analytical thin layer chromatography (TLC), performed on Aluminum silica gel 60 F₂₅₄ TLC plates, purchased from Merck, with visualization under UV light (254 nm). ¹HNMR spectra were determined on a two-channel Bruker AV-NEO NMR spectrometer operating at 11.7 T (500 MHz) and equipped with a 5 mm DCH cryoprobe in δ scale (ppm) and J (Hz) and referred to the deuterated solvent peak (DMSO-*d*₆ δ = 2.5 ppm). ¹³CNMR spectra were determined on the same instrument at 126 MHz and referred to the solvent peak (DMSO-*d*₆ δ = 39.52 ppm). All NMR datasets were acquired at 298 K unless otherwise stated. High resolution mass spectrometry (HRMS) was carried out using a Bruker MaXis Impact Time of Flight spectrophotometer, using electrospray ionization (ES+).

4.1.1. General synthetic procedures for indolin-2-one derivatives

The desired indolin-2-one derivatives were synthesized according to the previously reported procedures [39–43] and is illustrated as follows.

Step a: To a solution of 6-bromoindolin-2-one (**2**) (2.12 g, 10.0 mmol, 1.00 equiv) and 1*H*-pyrrole-2-carboxaldehyde (**3**) (0.95 g, 10.0 mmol, 1.00 equiv) in toluene (40 ml) was added catalytic amount of piperdine (200 μ l) and glacial acetic acid (200 μ l) and the reaction mixture was heated at 80°C for 2 h. Upon completion of the reaction as indicated by TLC, the mixture was cooled, evaporated, and the resulting residue was stirred with hexane, filtered, dried, and

purified by flash chromatography (DCM/Hexane 9:1) to yield the desired (Z)-3-((1H-pyrrol-2-yl)methylene)-6-bromoindolin-2-one (**4**) in 82% yield.

Step b: A solution of (Z)-3-((1H-pyrrol-2-yl)methylene)-6-bromoindolin-2-one (**4**) (289 mg, 1.00 mmol, 1.00 equiv) and the appropriate boronic acid (2.00 mmol, 2.00 equiv) in dioxane/water (4:1, 24 ml) was purged with nitrogen for 5 min then Pd tetrakis (23.0 mg, 0.02 mmol, 0.02 equiv) and K₂CO₃ (415 mg, 3.00 mmol, 3.00 equiv) were added and the reaction was refluxed under nitrogen for 6 hr. Upon completion of the reaction as indicated by TLC, the mixture was cooled, filtered using celite, evaporated, and the resulting residue was extracted with ethyl acetate. The organic layer was dried over anhydrous Na₂SO₄, evaporated, and the resulting residue was purified by flash chromatography to yield the desired final products (**1**, **5a-g**) and the amine intermediates (**5h,i**).

4.1.1.1. (Z)-3-((1H-pyrrol-2-yl)methylene)-6-(4-hydroxyphenyl)indolin-2-one (1) [31]. R_f = 0.25 (DCM/MeOH 9.8:0.2). Dark orange solid, yield 55%. ¹H NMR (501 MHz, DMSO-d₆) δ 13.32 (s, 1H), 10.95 (s, 1H), 9.56 (s, 1H), 7.73 (s, 1H), 7.65 (d, J = 8.0 Hz, 1H), 7.47 (dd, J = 2.0, 6.7 Hz, 2H), 7.36 (q, J = 2.0 Hz, 1H), 7.22 (dd, J = 1.6, 8.0 Hz, 1H), 7.04 (d, J = 1.4 Hz, 1H), 6.85 (dd, J = 2.0, 6.7 Hz, 2H), 6.83 (q, J = 1.7 Hz, 1H), 6.38 - 6.35 (1H, m). ¹³C NMR (126 MHz, DMSO-d₆) δ 170.0, 157.6, 140.1, 139.7, 131.6, 130.2, 128.1 (2C), 126.3, 126.0, 124.0, 120.6, 119.7, 119.4, 117.3, 116.2 (2C), 111.9, 107.4. HRMS exact mass of C₁₉H₁₄N₂O₂ (M+H)⁺: 303.1128 amu; found: 303.1119 amu.

4.1.1.2. (Z)-3-((1H-pyrrol-2-yl)methylene)-6-(3-hydroxyphenyl)indolin-2-one (5a). R_f = 0.30 (DCM/MeOH 9.8:0.2). Dark orange solid, yield 31%. ¹H NMR (501 MHz, DMSO-d₆) δ 13.33 (s, 1H), 10.99 (s, 1H), 9.52 (s, 1H), 7.77 (s, 1H), 7.69 (d, J = 7.9 Hz, 1H), 7.38 (q, J = 2.0 Hz, 1H), 7.27 - 7.23 (2H, m), 7.08 - 7.05 (2H, m), 7.02 (t, J = 2.0 Hz, 1H), 6.86 (q, J = 1.7 Hz, 1H), 6.78 - 6.75 (1H, m), 6.39 - 6.36 (1H, m). ¹³C NMR (126 MHz, DMSO-d₆) δ 169.9, 158.3, 142.3, 140.1, 139.6, 130.4, 130.2, 126.8, 126.3, 125.0, 120.9, 120.3, 119.4, 117.8, 117.1, 114.9, 113.7, 112.0, 108.0. HRMS exact mass of C₁₉H₁₄N₂O₂ (M+H)⁺: 303.1128 amu; found: 303.1122 amu.

4.1.1.3. (Z)-3-((1H-pyrrol-2-yl)methylene)-6-(4-hydroxy-3-methoxyphenyl)indolin-2-one (5b) [31]. R_f = 0.40 (DCM/MeOH 9.9:0.1). Orange solid, yield 49%. ¹H NMR (501 MHz, DMSO-d₆) δ 13.32 (s, 1H), 10.93 (s, 1H), 9.12 (s, 1H), 7.74 (s, 1H), 7.66 (d, J = 8.0 Hz, 1H), 7.36 (q, J = 2.1 Hz,

1H), 7.27 (dd, $J = 1.6, 8.0$ Hz, 1H), 7.17 (d, $J = 2.1$ Hz, 1H), 7.06 (dd, $J = 1.9, 8.5$ Hz, 2H), 6.86 (d, $J = 8.2$ Hz, 1H), 6.84 (q, $J = 1.8$ Hz, 1H), 6.37 (dt, $J = 1.9, 3.0$ Hz, 1H), 3.87 (s, 3H). **^{13}C NMR (126 MHz, DMSO- d_6)** δ 170.0, 148.4, 146.9, 140.1, 139.9, 132.3, 130.2, 126.3, 126.0, 124.1, 120.6, 120.0, 119.5, 119.4, 117.3, 116.4, 111.9, 111.1, 107.7, 56.1. **HRMS exact mass of $\text{C}_{20}\text{H}_{16}\text{N}_2\text{O}_3$ (M+H) $^+$:** 333.1233 amu; **found:** 333.1220 amu.

4.1.1.4. (Z)-4-(3-((1H-pyrrol-2-yl)methylene)-2-oxoindolin-6-yl)benzotrile (5c). $R_f = 0.30$ (DCM/MeOH 9.95:0.05). Orange solid, yield 81%. **^1H NMR (501 MHz, DMSO- d_6)** δ 13.34 (s, 1H), 11.08 (s, 1H), 7.91 (dd, $J = 4.0, 6.1$ Hz, 2H), 7.87 (dd, $J = 4.3, 4.3$ Hz, 2H), 7.85 (s, 1H), 7.77 (d, $J = 8.0$ Hz, 1H), 7.42 - 7.40 (2H, m), 7.19 (d, $J = 1.4$ Hz, 1H), 6.90 - 6.88 (1H, m), 6.39 (dt, $J = 1.9, 3.0$ Hz, 1H). **^{13}C NMR (126 MHz, DMSO- d_6)** δ 169.9, 145.3, 140.2, 137.2, 133.3 (2C), 130.2, 127.8 (2C), 127.7, 126.8, 126.4, 121.4, 120.9, 119.6, 119.4, 116.6, 112.2, 110.2, 108.3. **HRMS exact mass of $\text{C}_{20}\text{H}_{13}\text{N}_3\text{O}$ (M+H) $^+$:** 312.1131 amu; **found:** 312.1124 amu.

4.1.1.5. (Z)-3-(3-((1H-pyrrol-2-yl)methylene)-2-oxoindolin-6-yl)benzotrile (5d). $R_f = 0.20$ (DCM/MeOH 9.95:0.05). Dark orange solid, yield 65%. **^1H NMR (501 MHz, DMSO- d_6)** δ 13.34 (s, 1H), 11.09 (s, 1H), 8.15 (t, $J = 1.5$ Hz, 1H), 8.01 (ddd, $J = 1.1, 1.9, 8.0$ Hz, 1H), 7.84 (s, 1H), 7.81 (dt, $J = 2.5, 4.6$ Hz, 1H), 7.76 (d, $J = 8.0$ Hz, 1H), 7.68 - 7.64 (1H, m), 7.41 - 7.39 (2H, m), 7.19 (d, $J = 1.4$ Hz, 1H), 6.89 - 6.87 (1H, m), 6.40 - 6.38 (1H, m). **^{13}C NMR (126 MHz, DMSO- d_6)** δ 169.9, 142.0, 140.1, 137.1, 131.8, 131.3, 130.6, 130.6, 130.2, 127.5, 126.7, 126.0, 121.3, 120.7, 119.6, 119.3, 116.7, 112.6, 112.1, 108.3. **HRMS exact mass of $\text{C}_{20}\text{H}_{13}\text{N}_3\text{O}$ (M+Na) $^+$:** 334.0950 amu; **found:** 334.0946 amu.

4.1.1.6. (Z)-3-(((1H-pyrrol-2-yl)methylene)-6-(3-methoxyphenyl)indolin-2-one (5e). $R_f = 0.25$ (DCM). Orange solid, yield 43%. **^1H NMR (501 MHz, DMSO- d_6)** δ 13.34 (s, 1H), 10.99 (s, 1H), 7.79 (s, 1H), 7.71 (d, $J = 7.9$ Hz, 1H), 7.38 (q, $J = 5.3$ Hz, 2H), 7.33 (dd, $J = 1.6, 7.9$ Hz, 1H), 7.22 (d, $J = 7.7$ Hz, 1H), 7.17 (t, $J = 2.0$ Hz, 1H), 7.12 (d, $J = 1.4$ Hz, 1H), 6.94 (dd, $J = 1.9, 8.2$ Hz, 1H), 6.87 (t, $J = 1.7$ Hz, 1H), 6.38 (dt, $J = 1.9, 3.0$ Hz, 1H), 3.83 (s, 3H). **^{13}C NMR (126 MHz, DMSO- d_6)** δ 169.9, 160.2, 142.4, 140.1, 139.3, 130.5, 130.2, 126.9, 126.3, 125.2, 120.9, 120.6, 119.4, 119.4, 117.0, 113.5, 112.4, 112.0, 108.2, 55.6. **HRMS exact mass of $\text{C}_{20}\text{H}_{16}\text{N}_2\text{O}_2$ (M+H) $^+$:** 317.1284 amu; **found:** 317.1274 amu.

4.1.1.7. (Z)-3-((1H-pyrrol-2-yl)methylene)-6-(3-nitrophenyl)indolin-2-one (5f). $R_f = 0.35$ (DCM). Orange solid, yield 41%. $^1\text{H NMR}$ (501 MHz, DMSO- d_6) δ 13.34 (s, 1H), 11.07 (s, 1H), 8.42 (t, $J = 2.0$ Hz, 1H), 8.20 (ddd, $J = 0.9, 2.3, 8.2$ Hz, 1H), 8.15 (qd, $J = 0.9, 7.8$ Hz, 1H), 7.85 (s, 1H), 7.80 - 7.74 (2H, m), 7.45 (dd, $J = 1.7, 8.0$ Hz, 1H), 7.41 (q, $J = 2.0$ Hz, 1H), 7.22 (d, $J = 1.5$ Hz, 1H), 6.91 - 6.88 (1H, m), 6.39 (dt, $J = 1.9, 3.0$ Hz, 1H). $^{13}\text{C NMR}$ (126 MHz, DMSO- d_6) δ 169.9, 148.9, 142.4, 140.2, 136.8, 133.5, 131.0, 130.2, 127.6, 126.7, 126.2, 122.4, 121.4, 121.3, 120.8, 119.7, 116.6, 112.2, 108.3. HRMS exact mass of $\text{C}_{19}\text{H}_{13}\text{N}_3\text{O}_3$ (M+H) $^+$: 332.1029 amu; found: 332.1023 amu.

4.1.1.8. (Z)-3-((1H-pyrrol-2-yl)methylene)-6-(pyridin-4-yl)indolin-2-one (5g). $R_f = 0.35$ (DCM/MeOH 9.7:0.3). Orange solid, yield 15%. $^1\text{H NMR}$ (501 MHz, DMSO- d_6) δ 13.35 (s, 1H), 11.10 (s, 1H), 8.63 (d, $J = 4.8$ Hz, 2H), 7.86 (s, 1H), 7.79 (d, $J = 7.9$ Hz, 1H), 7.69 (d, $J = 4.7$ Hz, 2H), 7.47 (d, $J = 7.9$ Hz, 1H), 7.42 (s, 1H), 7.24 (s, 1H), 6.90 (s, 1H), 6.40 (d, $J = 1.9$ Hz, 1H). $^{13}\text{C NMR}$ (126 MHz, DMSO- d_6) δ 169.9, 150.7 (2C), 147.6, 140.2, 136.0, 130.2, 127.8, 126.9, 126.9, 121.5, 121.4 (2C), 120.6, 119.6, 116.6, 112.2, 108.0. HRMS exact mass of $\text{C}_{18}\text{H}_{13}\text{N}_3\text{O}$ (M+H) $^+$: 288.1131 amu; found: 288.1127 amu.

Step c: To an ice-cold solution of the appropriate amine (**5h,i**) (200 mg, 0.66 mmol, 1.00 equiv) in pyridine (10 ml) was added the appropriate acid chloride (0.79 mmol, 1.20 equiv) slowly and the reaction mixture was stirred at room temperature for 4 h. Upon completion of the reaction as indicated by TLC, the mixture was evaporated and purified by flash chromatography to yield the desired final products (**6a-e**).

4.1.1.9. (Z)-N-(4-(3-((1H-pyrrol-2-yl)methylene)-2-oxoindolin-6-yl)phenyl)acetamide (6a). $R_f = 0.30$ (DCM/MeOH 9.7:0.3). Dark orange solid, yield 71%. $^1\text{H NMR}$ (501 MHz, DMSO- d_6) δ 13.32 (s, 1H), 10.99 (s, 1H), 10.04 (s, 1H), 7.76 (s, 1H), 7.70 (d, $J = 6.2$ Hz, 1H), 7.67 (d, $J = 6.8$ Hz, 2H), 7.60 (d, $J = 8.7$ Hz, 2H), 7.37 (d, $J = 0.9$ Hz, 1H), 7.29 (dd, $J = 1.5, 8.0$ Hz, 1H), 7.10 (d, $J = 1.2$ Hz, 1H), 6.85 (t, $J = 1.7$ Hz, 1H), 6.37 (ddd, $J = 1.8, 1.8, 4.1$ Hz, 1H), 2.08 (s, 3H). $^{13}\text{C NMR}$ (126 MHz, DMSO- d_6) δ 170.0, 168.8, 140.1, 139.2, 139.1, 135.3, 130.2, 127.2 (2C), 126.6, 126.2, 124.6, 120.8, 120.0, 119.8 (2C), 119.5, 117.1, 112.0, 107.6, 24.5. HRMS exact mass of $\text{C}_{21}\text{H}_{17}\text{N}_3\text{O}_2$ (M+Na) $^+$: 366.1212 amu; found: 366.1209 amu.

4.1.1.10. (Z)-N-(3-(3-((1H-pyrrol-2-yl)methylene)-2-oxoindolin-6-yl)phenyl)acetamide (6b). $R_f = 0.20$ (DCM/MeOH 9.8:0.2). Orange solid, yield 62%. $^1\text{H NMR}$ (501 MHz, DMSO- d_6) δ 13.31 (s, 1H), 11.03 (s, 1H), 10.04 (s, 1H), 7.92 (s, 1H), 7.79 (s, 1H), 7.73 (d, $J = 7.7$ Hz, 1H), 7.55 (d, $J = 7.3$ Hz, 1H), 7.38 (d, $J = 8.6$ Hz, 2H), 7.32 (d, $J = 7.0$ Hz, 1H), 7.27 (d, $J = 7.6$ Hz, 1H), 7.09 (s, 1H), 6.87 (s, 1H), 6.38 (s, 1H), 2.08 (s, 3H). $^{13}\text{C NMR}$ (126 MHz, DMSO- d_6) δ 169.9, 168.9, 141.3, 140.4, 140.1, 139.3, 130.2, 129.8, 127.0, 126.4, 125.2, 121.6, 121.0, 120.3, 119.5, 118.4, 117.4, 117.0, 112.0, 107.9, 24.6. HRMS exact mass of $\text{C}_{21}\text{H}_{17}\text{N}_3\text{O}_2$ ($\text{M}+\text{H}$) $^+$: 344.1393 amu; found: 344.1387 amu.

4.1.1.11. (Z)-N-(4-(3-((1H-pyrrol-2-yl)methylene)-2-oxoindolin-6-yl)phenyl)cyclopropanecarboxamide (6c). $R_f = 0.35$ (DCM/MeOH 9.5:0.5). Dark orange solid, yield 67%. $^1\text{H NMR}$ (501 MHz, DMSO- d_6) δ 13.33 (s, 1H), 10.99 (s, 1H), 10.29 (s, 1H), 7.76 (s, 1H), 7.69 (t, $J = 4.2$ Hz, 3H), 7.60 (d, $J = 8.6$ Hz, 2H), 7.37 (s, 1H), 7.29 (d, $J = 7.9$ Hz, 1H), 7.10 (s, 1H), 6.85 (s, 1H), 6.37 (d, $J = 3.0$ Hz, 1H), 1.85 - 1.78 (1H, m), 0.82 (t, $J = 6.8$ Hz, 4H). $^{13}\text{C NMR}$ (126 MHz, DMSO- d_6) δ 172.1, 170.0, 140.1, 139.3, 139.1, 135.3, 130.2, 127.2 (2C), 126.6, 126.2, 124.6, 120.8, 120.0, 119.8 (2C), 119.5, 117.1, 112.0, 107.6, 15.1, 7.7 (2C). HRMS exact mass of $\text{C}_{23}\text{H}_{19}\text{N}_3\text{O}_2$ ($\text{M}+\text{H}$) $^+$: 370.1550 amu; found: 370.1546 amu.

4.1.1.12. (Z)-N-(4-(3-((1H-pyrrol-2-yl)methylene)-2-oxoindolin-6-yl)phenyl)benzamide (6d). $R_f = 0.30$ (DCM/MeOH 9.5:0.5). Orange solid, yield 55%. $^1\text{H NMR}$ (501 MHz, DMSO- d_6) δ 13.33 (s, 1H), 11.01 (s, 1H), 10.36 (s, 1H), 7.99 (d, $J = 7.2$ Hz, 2H), 7.90 (d, $J = 8.6$ Hz, 2H), 7.78 (s, 1H), 7.72 (d, $J = 8.0$ Hz, 1H), 7.68 (d, $J = 8.6$ Hz, 2H), 7.61 (t, $J = 7.3$ Hz, 1H), 7.56 (t, $J = 7.4$ Hz, 2H), 7.39 (s, 1H), 7.34 (q, $J = 3.1$ Hz, 1H), 7.14 (d, $J = 1.0$ Hz, 1H), 6.86 (s, 1H), 6.40 - 6.35 (1H, m). $^{13}\text{C NMR}$ (126 MHz, DMSO- d_6) δ 170.0, 166.0, 140.2, 139.1, 139.0, 136.0, 135.4, 132.1, 130.2, 128.9 (2C), 128.2 (2C), 127.1 (2C), 126.7, 126.2, 124.7, 121.1 (2C), 120.8, 120.1, 119.5, 117.1, 112.0, 107.7. HRMS exact mass of $\text{C}_{26}\text{H}_{19}\text{N}_3\text{O}_2$ ($\text{M}+\text{H}$) $^+$: 406.1550 amu; found: 406.1550 amu.

4.1.1.13. Ethyl (Z)-(4-(3-((1H-pyrrol-2-yl)methylene)-2-oxoindolin-6-yl)phenyl)carbamate (6e). $R_f = 0.30$ (DCM/MeOH 9.7:0.3). Orange solid, yield 73%. $^1\text{H NMR}$ (501 MHz, DMSO- d_6) δ 13.32 (s, 1H), 10.98 (s, 1H), 9.74 (s, 1H), 7.76 (s, 1H), 7.69 (d, $J = 7.1$ Hz, 1H), 7.58 (d, $J = 5.7$ Hz, 4H), 7.37 (s, 1H), 7.28 (d, $J = 6.9$ Hz, 1H), 7.09 (s, 1H), 6.87 (s, 1H), 6.37 (s, 1H), 4.15 (d, $J = 6.4$ Hz, 2H), 1.25 (s, 3H). $^{13}\text{C NMR}$ (126 MHz, DMSO- d_6) δ 170.0, 154.0, 140.1, 139.1 (2C), 134.7, 130.2, 127.3 (2C),

126.6, 126.2, 124.5, 120.7, 119.9, 119.5, 119.0 (2C), 117.2, 112.0, 107.6, 60.7, 15.0. **HRMS exact mass of C₂₂H₁₉N₃O₃ (M+H)⁺**: 374.1499 amu; **found**: 374.1492 amu.

Step d: To an ice-cold solution of the amine derivative (**5h**) (200 mg, 0.66 mmol, 1.00 equiv) in pyridine (10 ml) was added benzenesulfonyl chloride (141 mg, 102 μ l, 0.79 mmol, 1.20 equiv) slowly and the reaction mixture was stirred at room temperature for 24 h. Upon completion of the reaction as indicated by TLC, the mixture was evaporated and purified by flash chromatography to yield the desired final product (**7**).

4.1.1.14. (Z)-N-(4-(3-((1H-pyrrol-2-yl)methylene)-2-oxoindolin-6-yl)phenyl)benzenesulfonamide (7). R_f = 0.30 (DCM/MeOH 9.9:0.1). Reddish orange solid, yield 57%. **¹H NMR (501 MHz, DMSO-d₆)** δ 13.31 (s, 1H), 10.98 (s, 1H), 10.43 (s, 1H), 7.81 (t, J = 4.3 Hz, 2H), 7.76 (s, 1H), 7.67 (d, J = 8.0 Hz, 1H), 7.65 - 7.60 (1H, m), 7.59 (d, J = 6.4 Hz, 1H), 7.56 (q, J = 2.7 Hz, 1H), 7.54 (d, J = 8.7 Hz, 2H), 7.37 (d, J = 1.0 Hz, 1H), 7.23 (q, J = 3.2 Hz, 1H), 7.19 (d, J = 8.6 Hz, 2H), 7.03 (d, J = 1.3 Hz, 1H), 6.84 (t, J = 1.7 Hz, 1H), 6.38 - 6.35 (1H, m). **¹³C NMR (126 MHz, DMSO-d₆)** δ 169.9, 140.1 (2C), 138.5, 137.5, 136.4, 133.4, 130.2, 129.8 (2C), 127.7 (2C), 127.1 (2C), 126.8, 126.3, 124.8, 120.9, 120.7 (2C), 120.0, 119.5, 117.0, 112.0, 107.7. **HRMS exact mass of C₂₅H₁₉N₃O₃S (M+H)⁺**: 440.1074 amu; **found**: 440.1067 amu.

Step e: To a solution of the amine derivative (**5h**) (200 mg, 0.66 mmol, 1.00 equiv) in dry THF (20 ml) was added triphosgene (167 mg, 0.66 mmol, 1.00 equiv) and the reaction mixture was purged and refluxed under nitrogen for 2 h. Upon the reaction completion as indicated by TLC the solution was concentrated under reduced pressure. The resulting residue was dissolved in dry THF (20 ml) and the appropriate amine (0.99 mmol, 1.50 equiv) and DIPEA (168 mg, 226 μ l, 1.30 mmol, 2.00 equiv) were added, and the reaction mixture was refluxed under nitrogen for 24 h. Upon completion of the reaction as indicated by TLC, the solution was concentrated, and the residue was purified by flash chromatography to give the desired final products (**8a,b**).

4.1.1.15. (Z)-1-(4-(3-((1H-pyrrol-2-yl)methylene)-2-oxoindolin-6-yl)phenyl)-3-cyclopropylurea (8a). R_f = 0.20 (DCM/MeOH 9.7:0.3). Orange solid, yield 44%. **¹H NMR (501 MHz, DMSO-d₆)** δ 13.32 (s, 1H), 10.97 (s, 1H), 8.41 (s, 1H), 7.75 (s, 1H), 7.68 (d, J = 8.0 Hz, 1H), 7.54 (d, J = 8.8 Hz, 2H), 7.50 (d, J = 8.8 Hz, 2H), 7.37 (d, J = 0.9 Hz, 1H), 7.27 (q, J = 3.1 Hz, 1H), 7.08 (d, J = 1.2 Hz, 1H),

6.84 (t, $J = 1.6$ Hz, 1H), 6.42 (d, $J = 2.3$ Hz, 1H), 6.39 - 6.35 (1H, m), 2.58 - 2.54 (1H, m), 0.68 - 0.62 (2H, m), 0.45 - 0.40 (2H, m). ^{13}C NMR (126 MHz, DMSO- d_6) δ 170.0, 156.4, 140.3, 140.1, 139.3, 133.5, 130.2, 127.2 (2C), 126.5, 126.1, 124.3, 120.7, 119.8, 119.5, 118.7 (2C), 117.2, 111.9, 107.5, 22.9, 6.9 (2C). HRMS exact mass of $\text{C}_{23}\text{H}_{20}\text{N}_4\text{O}_2$ ($\text{M}+\text{H}$) $^+$: 385.1659 amu; found: 385.1655 amu.

4.1.1.16. (Z)-1-(4-(3-((1H-pyrrol-2-yl)methylene)-2-oxoindolin-6-yl)phenyl)-3-(3-tolyl)urea (8b). $R_f = 0.35$ (DCM/MeOH 9.7:0.3). Orange solid, yield 61%. ^1H NMR (501 MHz, DMSO- d_6) δ 13.33 (s, 1H), 10.99 (s, 1H), 8.77 (s, 1H), 8.62 (s, 1H), 7.76 (s, 1H), 7.69 (d, $J = 7.9$ Hz, 1H), 7.60 (d, $J = 8.5$ Hz, 2H), 7.55 (d, $J = 8.4$ Hz, 2H), 7.37 (s, 1H), 7.33 (s, 1H), 7.30 (d, $J = 7.9$ Hz, 1H), 7.25 (d, $J = 7.9$ Hz, 1H), 7.17 (t, $J = 7.7$ Hz, 1H), 7.10 (s, 1H), 6.85 (s, 1H), 6.81 (d, $J = 7.2$ Hz, 1H), 6.37 (s, 1H), 2.29 (s, 3H). ^{13}C NMR (126 MHz, DMSO- d_6) δ 170.0, 152.9, 140.2, 140.0, 139.7, 139.2, 138.4, 134.2, 130.2, 129.1, 127.3 (2C), 126.5, 126.1, 124.4, 123.1, 120.7, 119.9, 119.5, 119.2, 119.0 (2C), 117.2, 115.9, 111.9, 107.5, 21.7. HRMS exact mass of $\text{C}_{27}\text{H}_{22}\text{N}_4\text{O}_2$ ($\text{M}+\text{H}$) $^+$: 435.1815 amu; found: 435.1819 amu.

4.2. Biological evaluation

4.2.1. Kinase Inhibition Assays

The kinase inhibition assays were performed using the SelectScreen kinase profiling service of ThermoFisher Scientific. Abl1, ALK, AURKA, AURKB, Chk1, JAK2, JAK3, VEGFR2, PDGFR β , and RET kinases inhibition was determined using Z'-LYTE assay protocol, while LRRK2 kinase inhibition was determined using Adapta assay protocol. All data were obtained by double testing and the IC₅₀ values were calculated using nonlinear regression with normalized dose-response fit using Prism GraphPad software.

4.2.2. Reagents, and antibodies

ROCHE Complete™ EDTA-free Protease Inhibitor Cocktail (Catalog.No.11836170001) was purchased from Sigma Aldrich. Bio-Rad DC™ Protein Assay (Catalog.No.500-0114) was purchased from Bio-Rad. Primary antibodies against phosphorylated Aurora kinase B (Thr232), phosphorylated histone 3 (S10), and total histone 3 were purchased from Cell Signaling Technology and Abcam. Anti-vinculin was purchased from Sigma Aldrich. Sunitinib malate was

purchased from Selleckchem. All the other chemicals and solvents were of the highest commercially available grade.

4.2.3. Cancer and normal cell lines and cell culture

Human breast cancer cell line MDA-MB-468, was obtained from ATCC. MDA-MB-468 cells were cultured in Ham's F-12/DMEM (1:1 ratio) media supplemented with 2 mM L-glutamine, 10% FBS, and 1% penicillin-streptomycin. Normal rat cardiomyoblast (H9c2) and murine hepatocyte (BNL) cell lines were cultured in DMEM media supplemented with 10% FBS, 2 mM L-glutamine and 1% penicillin-streptomycin. Cells were maintained in a humidified tissue culture incubator at 37°C with 5% CO₂. All cell lines were tested for mycoplasma contamination and resulted negative before being used in further experiments.

4.2.4. Cell viability assay

To determine the effect of the synthesized compounds on their viability, MDA-MB-468, H9c2 and BNL cells were treated with varying concentrations of the synthesized compounds for the indicated time points. Cell viability was determined using a Cell Titer-Glo™ Luminescent Cell Viability assay (Promega Corporation, USA) which quantifies cellular ATP levels as an indicator of metabolically active cells [60]. Luminescence was measured using Glomax™ Multi-Detection System (Promega Corporation, USA).

4.2.5. Clonogenic assay

MDA-MB-468 cells were seeded in 6-well plates (250 cells/well) overnight and then treated with the indicated concentrations of compounds **6e** or **8a**. Fourteen days later, colonies were fixed and stained using 0.5% crystal violet in 50/50 methanol/water for 30 min. Six-well plates were then rinsed with water and left for drying at room temperature and colonies were counted.

4.2.6. Cell cycle analysis

Flowcytometric DNA ploidy analysis of MDA-MB-468 cells treated with vehicle or compounds **6e** or **8a** was performed as previously described [61]. Cell cycle analysis using propidium iodide (50 µg/ml) was performed using FACS Celesta and analyzed using FlowJo software.

4.2.7. Quantification of cell death

After MDA-MB-468 cells were treated as indicated, cells were washed in PBS (pH 7.2), and then stained with propidium iodide. Cell fluorescence was then measured using a flow cytometer (FACSCalibur; Becton Dickinson, CA) and analyzed using FlowJo software as previously described [60].

4.2.8. Immunoblot analysis

Following their treatment with the indicated concentration of compound **8a**, MDA-MB-468 cells were harvested and lysed in SDS lysis buffer comprising ROCHE Complete™ EDTA-free Protease Inhibitor Cocktail as previously described [62]. The protein content of cell lysates was assessed using Bio-Rad protein DC assay and then resolved on 12% SDS–PAGE and transferred to nitrocellulose membrane using a wet transfer system (Bio-Rad). The membrane was then blocked with 5% skimmed milk in TBST for 1 h at room temperature. The membrane was incubated with the indicated primary antibodies in TBST (containing 5% skimmed milk) at 4°C overnight. After three washing cycles with TBST, the membrane was blotted with horseradish peroxidase-conjugated secondary antibody at room temperature for 1 h. The membrane was then washed with TBST thrice. Protein bands were detected with a Chemiluminescence western blot detection kit (Amersham Pharmacia Biotech, Piscataway, NJ, USA).

4.2.9. Statistical Analysis

Analysis of the data was carried out using GraphPad InStat (Version 2) as follows; Data are presented as mean ± standard deviation (SD). One way analysis of variance (ANOVA) followed by Dunnett test for post-hoc analysis was used for multiple comparisons (> two treatment groups). Statistical significance was acceptable at P value <0.05. Graphs were presented using Graphpad

Prism software program (GraphPad software incorporated, version 5). Median inhibitory concentrations (IC₅₀) values were obtained from Sigmoidal dose-response (Variable slope) curves using GraphPad Prism software.

4.3. Molecular modeling

Molecular docking of **1** and target compounds was performed using Discovery Studio® CDOCKER protocol (version 2.5, Accelrys, Inc., San Diego, CA). The X-ray crystal structure of Aurora B kinase enzyme was obtained from PDB server (PDB ID: 2C2V). The protein structure was prepared according to the standard protein preparation procedure integrated in Accelrys' Discovery Studio 2.5, which involved adding hydrogen atoms, completing the missing loops, and assigning force field parameters. CHARMM force field was used for simulation studies and then the protein structure was minimized using 1000 iterations of steepest descent minimization algorithm. The ligands were drawn using the sketching tools of Accelrys' Discovery Studio and they were prepared for docking by adding hydrogen atoms and partial charges using the Momany-Rone method. For docking, the CDOCKER protocol was used. The binding site was defined by the residues within 10 Å distance from the co-crystallized ligand. The default values of CDOCKER were used. Ten different docking solutions were generated and visually inspected for selection of the best binding mode. Docking scores for the best binding poses were reported using -CDOCKER_INTERACTION_ENERGY. The results were viewed using PyMOL software (v2.3, <https://pymol.org/2/>).

Acknowledgment

AKA has been awarded a fellowship from Fondazione IEO-CCM. SNM has been awarded a PhD scholarship at University of Leeds funded by the Newton-Mosharafa Fund jointly offered by the British Council and the Ministry of Higher Education of the Arab Republic of Egypt. We thank Dr Jeanine Williams (School of Chemistry, University of Leeds) for conducting the HPLC purity determination assays.

Conflicts of interest

The authors declare no competing financial interest.

Appendix A. Supplementary material

Supplementary data to this article can be found online at <https://doi.org/xxxxxxx>.

Abbreviations

Abl1, Abelson tyrosine protein kinase 1; ALK, Anaplastic lymphoma kinase; AURKA, Aurora kinase A; AURKB, Aurora kinase B; Chk1, Checkpoint kinase 1; FACS, Fluorescence-activated cell sorting; JAK2, Janus Kinase 2; JAK3, Janus Kinase 3; LRRK2, Leucine-rich repeat kinase 2; PDGFR β , Platelet-derived growth factor receptor beta; PI, Propidium iodide; RET, Rearranged during transfection tyrosine kinase; VEGFR2, Vascular endothelial growth factor receptor 2.

References

- [1] J. Fu, M. Bian, Q. Jiang, C. Zhang, Roles of aurora kinases in mitosis and tumorigenesis, *Mol. Cancer Res.* 5 (2007) 1–10. doi:10.1158/1541-7786.MCR-06-0208.
- [2] D. Ducat, Y. Zheng, Aurora kinases in spindle assembly and chromosome segregation, *Exp. Cell Res.* 301 (2004) 60–67. doi:10.1016/j.yexcr.2004.08.016.
- [3] B.A.A. Weaver, D.W. Cleveland, Decoding the links between mitosis, cancer, and chemotherapy: The mitotic checkpoint, adaptation, and cell death, *Cancer Cell.* 8 (2005) 7–12. doi:10.1016/j.ccr.2005.06.011.
- [4] A. Tang, K. Gao, L. Chu, R. Zhang, J. Yang, J. Zheng, Aurora kinases: Novel therapy targets in cancers, *Oncotarget.* 8 (2017) 23937–23954. doi:10.18632/oncotarget.14893.
- [5] R.D. Carvajal, A. Tse, G.K. Schwartz, Aurora kinases: New targets for cancer therapy, *Clin. Cancer Res.* 12 (2006) 6869–6875. doi:10.1158/1078-0432.CCR-06-1405.
- [6] D. Galetta, L. Cortes-Dericks, Promising Therapy in Lung Cancer: Spotlight on Aurora Kinases, *Cancers (Basel).* 12 (2020) 1–15. doi:10.3390/CANCERS12113371.
- [7] V. Bavetsias, S. Linardopoulos, Aurora kinase inhibitors: Current status and outlook, *Front.*

- Oncol. 5 (2015) 278. doi:10.3389/fonc.2015.00278.
- [8] A.C. Borisa, H.G. Bhatt, A comprehensive review on Aurora kinase: Small molecule inhibitors and clinical trial studies, *Eur. J. Med. Chem.* 140 (2017) 1–19. doi:10.1016/j.ejmech.2017.08.045.
- [9] N.A. Borah, M.M. Reddy, Aurora Kinase B Inhibition: A Potential Therapeutic Strategy for Cancer, *Molecules.* 26 (2021) 1981. doi:10.3390/molecules26071981.
- [10] M. Kollareddy, D. Zheleva, P. Dzubak, P.S. Brahmshatriya, M. Lepsik, M. Hajduch, Aurora kinase inhibitors: Progress towards the clinic, *Invest. New Drugs.* 30 (2012) 2411–2432. doi:10.1007/s10637-012-9798-6.
- [11] D. Bebbington, H. Binch, J.D. Charrier, S. Everitt, D. Fraysse, J. Golec, D. Kay, R. Knechtel, C. Mak, F. Mazzei, A. Miller, M. Mortimore, M. O'Donnell, S. Patel, F. Pierard, J. Pinder, J. Pollard, S. Ramaya, D. Robinson, A. Rutherford, J. Studley, J. Westcott, The discovery of the potent aurora inhibitor MK-0457 (VX-680), *Bioorganic Med. Chem. Lett.* 19 (2009) 3586–3592. doi:10.1016/j.bmcl.2009.04.136.
- [12] S. Howard, V. Berdini, J.A. Boulstridge, M.G. Carr, D.M. Cross, J. Curry, L.A. Devine, T.R. Early, L. Fazal, A.L. Gill, M. Heathcote, S. Maman, J.E. Matthews, R.L. McMenamin, E.F. Navarro, M.A. O'Brien, M. O'Reilly, D.C. Rees, M. Reule, D. Tisi, G. Williams, M. Vinković, P.G. Wyatt, Fragment-based discovery of the pyrazol-4-yl urea (AT9283), a multitargeted kinase inhibitor with potent aurora kinase activity, *J. Med. Chem.* 52 (2009) 379–388. doi:10.1021/jm800984v.
- [13] C. Ditchfield, V.L. Johnson, A. Tighe, R. Ellston, C. Haworth, T. Johnson, A. Mortlock, N. Keen, S.S. Taylor, Aurora B couples chromosome alignment with anaphase by targeting BubR1, Mad2, and Cenp-E to kinetochores, *J. Cell Biol.* 161 (2003) 267–280. doi:10.1083/jcb.200208091.
- [14] S. Hauf, R.W. Cole, S. LaTerra, C. Zimmer, G. Schnapp, R. Walter, A. Heckel, J. Van Meel, C.L. Rieder, J.M. Peters, The small molecule Hesperadin reveals a role for Aurora B in correcting kinetochore-microtubule attachment and in maintaining the spindle assembly

- checkpoint, *J. Cell Biol.* 161 (2003) 281–294. doi:10.1083/jcb.200208092.
- [15] A.A. Mortlock, K.M. Foote, N.M. Heron, F.H. Jung, G. Pasquet, J.J.M. Lohmann, N. Warin, F. Renaud, C. De Savi, N.J. Roberts, T. Johnson, C.B. Dousson, G.B. Hill, D. Perkins, G. Hatter, R.W. Wilkinson, S.R. Wedge, S.P. Heaton, R. Odedra, N.J. Keen, C. Crafter, E. Brown, K. Thompson, S. Brightwell, L. Khatri, M.C. Brady, S. Kearney, D. McKillop, S. Rhead, T. Parry, S. Green, Discovery, synthesis, and in vivo activity of a new class of pyrazoloquinazolines as selective inhibitors of aurora B kinase, *J. Med. Chem.* 50 (2007) 2213–2224. doi:10.1021/jm061335f.
- [16] N.R. Lakkaniga, L. Zhang, B. Belachew, N. Gunaganti, B. Frett, H. Yu Li, Discovery of SP-96, the first non-ATP-competitive Aurora Kinase B inhibitor, for reduced myelosuppression, *Eur. J. Med. Chem.* 203 (2020) 112589. doi:10.1016/j.ejmech.2020.112589.
- [17] Chieffi P., Aurora B: A new promising therapeutic target in cancer., *Intractable Rare Dis. Res.* 7 (2018) 141–144. doi:10.5582/IRDR.2018.01018.
- [18] G.S. Papaetis, K.N. Syrigos, Sunitinib: A multitargeted receptor tyrosine kinase inhibitor in the era of molecular cancer therapies, *BioDrugs.* 23 (2009) 377–389. doi:10.2165/11318860-000000000-00000.
- [19] D. Kitagawa, K. Yokota, M. Gouda, Y. Narumi, H. Ohmoto, E. Nishiwaki, K. Akita, Y. Kirii, Activity-based kinase profiling of approved tyrosine kinase inhibitors, *Genes to Cells.* 18 (2013) 110–122. doi:10.1111/gtc.12022.
- [20] Y. Han, W. Dong, Q. Guo, X. Li, L. Huang, The importance of indole and azaindole scaffold in the development of antitumor agents, *Eur. J. Med. Chem.* 203 (2020) 112506. doi:10.1016/j.ejmech.2020.112506.
- [21] P. Dhokne, A.P. Sakla, N. Shankaraiah, Structural insights of oxindole based kinase inhibitors as anticancer agents: Recent advances, *Eur. J. Med. Chem.* 216 (2021) 113334. doi:10.1016/j.ejmech.2021.113334.
- [22] Z. Zhao, H. Wu, L. Wang, Y. Liu, S. Knapp, Q. Liu, N.S. Gray, Exploration of type II binding

- mode: A privileged approach for kinase inhibitor focused drug discovery?, *ACS Chem. Biol.* 9 (2014) 1230–1241. doi:10.1021/cb500129t.
- [23] F. Miljković, J. Bajorath, Exploring Selectivity of Multikinase Inhibitors across the Human Kinome, *ACS Omega.* 3 (2018) 1147–1153. doi:10.1021/acsomega.7b01960.
- [24] K.S. Bhullar, N.O. Lagarón, E.M. McGowan, I. Parmar, A. Jha, B.P. Hubbard, H.P.V. Rupasinghe, Kinase-targeted cancer therapies: Progress, challenges and future directions, *Mol. Cancer.* 17 (2018) 1–20. doi:10.1186/s12943-018-0804-2.
- [25] K. Godl, O.J. Gruss, J. Eickhoff, J. Wissing, S. Blencke, M. Weber, H. Degen, D. Brehmer, L. Orfi, Z. Horváth, G. Kéri, S. Müller, M. Cotten, A. Ullrich, H. Daub, Proteomic characterization of the angiogenesis inhibitor SU6668 reveals multiple impacts on cellular kinase signaling, *Cancer Res.* 65 (2005) 6919–6926. doi:10.1158/0008-5472.CAN-05-0574.
- [26] M.S. Phadke, P. Sini, K.S.M. Smalley, The novel ATP-competitive MEK/aurora kinase inhibitor BI-847325 overcomes acquired BRAF inhibitor resistance through suppression of Mcl-1 and MEK expression, *Mol. Cancer Ther.* 14 (2015) 1354–1364. doi:10.1158/1535-7163.MCT-14-0832.
- [27] J. Bogusz, K. Zrubek, K.P. Rembacz, P. Grudnik, P. Golik, M. Romanowska, B. Wladyka, G. Dubin, Structural analysis of PIM1 kinase complexes with ATP-competitive inhibitors, *Sci. Rep.* 7 (2017). doi:10.1038/s41598-017-13557-z.
- [28] K.G. Pike, Inhibitors of the fibroblast growth factor receptor, in: *Top. Med. Chem.*, Springer Verlag, 2018: pp. 141–187. doi:10.1007/7355_2017_13.
- [29] M. Zachari, J.M. Rainard, G.C. Pandarakalam, L. Robinson, J. Gillespie, M. Rajamanickam, V. Hamon, A. Morrison, I.G. Ganley, S.P. McElroy, The identification and characterisation of autophagy inhibitors from the published kinase inhibitor sets, *Biochem. J.* 477 (2020) 801–814. doi:10.1042/BCJ20190846.
- [30] M. Davies, M. Nowotka, G. Papadatos, N. Dedman, A. Gaulton, F. Atkinson, L. Bellis, J.P. Overington, ChEMBL web services: Streamlining access to drug discovery data and utilities,

- Nucleic Acids Res. 43 (2015) W612–W620. doi:10.1093/nar/gkv352.
- [31] N.H. Lin, P. Xia, P. Kovar, C. Park, Z. Chen, H. Zhang, S.H. Rosenberg, H.L. Sham, Synthesis and biological evaluation of 3-ethylidene-1,3-dihydro-indol-2-ones as novel checkpoint 1 inhibitors, *Bioorganic Med. Chem. Lett.* 16 (2006) 421–426. doi:10.1016/j.bmcl.2005.09.064.
- [32] J. Bajorath, Compound data mining for drug discovery, in: *Methods Mol. Biol.*, Humana Press Inc., 2017: pp. 247–256. doi:10.1007/978-1-4939-6613-4_14.
- [33] F. Milletti, J.C. Hermann, Targeted kinase selectivity from kinase profiling data, *ACS Med. Chem. Lett.* 3 (2012) 383–386. doi:10.1021/ml300012r.
- [34] S.H. Henderson, F. Sorrell, J. Bennett, M.T. Hanley, S. Robinson, I. Hopkins Navratilova, J.M. Elkins, S.E. Ward, Mining Public Domain Data to Develop Selective DYRK1A Inhibitors, *ACS Med. Chem. Lett.* 11 (2020) 1620–1626. doi:10.1021/acsmchemlett.0c00279.
- [35] C. Bournez, F. Carles, G. Peyrat, S. Aci-Sèche, S. Bourg, C. Meyer, P. Bonnet, Comparative Assessment of Protein Kinase Inhibitors in Public Databases and in PKIDB, *Molecules.* 25 (2020) 3226. doi:10.3390/molecules25143226.
- [36] A. Gaulton, A. Hersey, M.L. Nowotka, A. Patricia Bento, J. Chambers, D. Mendez, P. Mutowo, F. Atkinson, L.J. Bellis, E. Cibrian-Uhalte, M. Davies, N. Dedman, A. Karlsson, M.P. Magarinos, J.P. Overington, G. Papadatos, I. Smit, A.R. Leach, The ChEMBL database in 2017, *Nucleic Acids Res.* 45 (2017) D945–D954. doi:10.1093/nar/gkw1074.
- [37] Claudio Viegas-Junior, Eliezer J. Barreiro, Carlos Alberto Manssour Fraga, Molecular Hybridization: A Useful Tool in the Design of New Drug Prototypes, *Curr. Med. Chem.* 14 (2007) 1829–1852. doi:10.2174/092986707781058805.
- [38] V. Ivasiv, C. Albertini, A.E. Gonçalves, M. Rossi, M.L. Bolognesi, Molecular Hybridization as a Tool for Designing Multitarget Drug Candidates for Complex Diseases, *Curr. Top. Med. Chem.* 19 (2019) 1694–1711. doi:10.2174/1568026619666190619115735.
- [39] C.J. Matheson, K.A. Casalvieri, D.S. Backos, M. Minhajuddin, C.T. Jordan, P. Reigan,

- Substituted oxindol-3-ylidenes as AMP-activated protein kinase (AMPK) inhibitors, *Eur. J. Med. Chem.* 197 (2020) 112316. doi:10.1016/j.ejmech.2020.112316.
- [40] C. Li, Y. Liu, S. Wu, G. Han, J. Tu, G. Dong, N. Liu, C. Sheng, Targeting fungal virulence factor by small molecules: Structure-based discovery of novel secreted aspartic protease 2 (SAP2) inhibitors, *Eur. J. Med. Chem.* 201 (2020) 112515. doi:10.1016/j.ejmech.2020.112515.
- [41] D. Bensinger, D. Stubba, A. Cremer, V. Kohl, T. Waßmer, J. Stuckert, V. Engemann, K. Stegmaier, K. Schmitz, B. Schmidt, Virtual Screening Identifies Irreversible FMS-like Tyrosine Kinase 3 Inhibitors with Activity toward Resistance-Confering Mutations, *J. Med. Chem.* 62 (2019) 2428–2446. doi:10.1021/acs.jmedchem.8b01714.
- [42] W.S. Palmer, G. Poncet-Montange, G. Liu, A. Petrocchi, N. Reyna, G. Subramanian, J. Theroff, A. Yau, M. Kost-Alimova, J.P. Bardenhagen, E. Leo, H.E. Shepard, T.N. Tieu, X. Shi, Y. Zhan, S. Zhao, M.C. Barton, G. Draetta, C. Toniatti, P. Jones, M. Geck Do, J.N. Andersen, Structure-Guided Design of IACS-9571, a Selective High-Affinity Dual TRIM24-BRPF1 Bromodomain Inhibitor, *J. Med. Chem.* 59 (2016) 1440–1454. doi:10.1021/acs.jmedchem.5b00405.
- [43] E.M.E. Dokla, C.S. Fang, K.A.M. Abouzid, C.S. Chen, 1,2,4-Oxadiazole derivatives targeting EGFR and c-Met degradation in TKI resistant NSCLC, *Eur. J. Med. Chem.* 182 (2019) 111607. doi:10.1016/j.ejmech.2019.111607.
- [44] Z.A. Knight, H. Lin, K.M. Shokat, Targeting the cancer kinome through polypharmacology, *Nat. Rev. Cancer.* 10 (2010) 130–137. doi:10.1038/nrc2787.
- [45] F. Broekman, Tyrosine kinase inhibitors: Multi-targeted or single-targeted?, *World J. Clin. Oncol.* 2 (2011) 80. doi:10.5306/wjco.v2.i2.80.
- [46] M. Kawai, A. Nakashima, S. Kamada, U. Kikkawa, Midostaurin preferentially attenuates proliferation of triple-negative breast cancer cell lines through inhibition of Aurora kinase family, *J. Biomed. Sci.* 22 (2015). doi:10.1186/s12929-015-0150-2.
- [47] C.P. Gully, F. Zhang, J. Chen, J.A. Yeung, G. Velazquez-Torres, E. Wang, S.C.J. Yeung, M.H.

- Lee, Antineoplastic effects of an Aurora B kinase inhibitor in breast cancer, *Mol. Cancer*. 9 (2010) 1–13. doi:10.1186/1476-4598-9-42.
- [48] N. Ghimirey, C. Steele, B.J. Czerniecki, G.K. Koski, L.E. Showalter, Sunitinib Combined with Th1 Cytokines Potentiates Apoptosis in Human Breast Cancer Cells and Suppresses Tumor Growth in a Murine Model of HER-2pos Breast Cancer, *Int. J. Breast Cancer*. 2021 (2021) 1–12. doi:10.1155/2021/8818393.
- [49] E. Chinchar, K.L. Makey, J. Gibson, F. Chen, S.A. Cole, G.C. Megason, S. Vijayakumar, L. Miele, J.W. Gu, Sunitinib significantly suppresses the proliferation, migration, apoptosis resistance, tumor angiogenesis and growth of triple-negative breast cancers but increases breast cancer stem cells, *Vasc. Cell*. 6 (2014) 12. doi:10.1186/2045-824X-6-12.
- [50] J. Yang, T. Ikezoe, C. Nishioka, T. Tasaka, A. Taniguchi, Y. Kuwayama, N. Komatsu, K. Bandobashi, K. Togitani, H.P. Koeffler, H. Taguchi, A. Yokoyama, AZD1152, a novel and selective aurora B kinase inhibitor, induces growth arrest, apoptosis, and sensitization for tubulin depolymerizing agent or topoisomerase II inhibitor in human acute leukemia cells in vitro and in vivo, *Blood*. 110 (2007) 2034–2040. doi:10.1182/blood-2007-02-073700.
- [51] O. Gautschi, J. Heighway, P.C. Mack, P.R. Purnell, P.N. Lara, D.R. Gandara, Aurora kinases as anticancer drug targets, *Clin. Cancer Res*. 14 (2008) 1639–1648. doi:10.1158/1078-0432.CCR-07-2179.
- [52] M. Trakala, G. Fernández-Miranda, I.P. De Castro, C. Heeschen, M. Malumbres, Aurora B prevents delayed DNA replication and premature mitotic exit by repressing p21Cip1, *Cell Cycle*. 12 (2013) 1030–1041. doi:10.4161/cc.24004.
- [53] Y. Yasui, T. Urano, A. Kawajiri, K.I. Nagata, M. Tatsuka, H. Saya, K. Furukawa, T. Takahashi, I. Izawa, M. Inagaki, Autophosphorylation of a Newly Identified Site of Aurora-B Is Indispensable for Cytokinesis, *J. Biol. Chem*. 279 (2004) 12997–13003. doi:10.1074/jbc.M311128200.
- [54] H. Goto, Y. Yasui, E.A. Nigg, M. Inagaki, Aurora-B phosphorylates Histone H3 at serine28 with regard to the mitotic chromosome condensation, *Genes to Cells*. 7 (2002) 11–17.

doi:10.1046/j.1356-9597.2001.00498.x.

- [55] T. Hirota, J.J. Lipp, B.H. Toh, J.M. Peters, Histone H3 serine 10 phosphorylation by Aurora B causes HP1 dissociation from heterochromatin, *Nature*. 438 (2005) 1176–1180. doi:10.1038/nature04254.
- [56] A. Aqsa, S. Droubi, S. Amarnath, H. Al-Moussawi, J. Abergel, Sunitinib-Induced Acute Liver Failure, *Case Rep. Gastroenterol.* 15 (2021) 17–21. doi:10.1159/000511249.
- [57] A.K. Abdel-Aziz, E.M. Mantawy, R.S. Said, R. Helwa, The tyrosine kinase inhibitor, sunitinib malate, induces cognitive impairment in vivo via dysregulating VEGFR signaling, apoptotic and autophagic machineries, *Exp. Neurol.* 283 (2016) 129–141. doi:10.1016/j.expneurol.2016.06.004.
- [58] T.F. Chu, M.A. Rupnick, R. Kerkela, S.M. Dallabrida, D. Zurakowski, L. Nguyen, K. Woulfe, E. Pravda, F. Cassiola, J. Desai, S. George, J.A. Morgan, D.M. Harris, N.S. Ismail, J.H. Chen, F.J. Schoen, A.D. Van den Abbeele, G.D. Demetri, T. Force, M.H. Chen, Cardiotoxicity associated with tyrosine kinase inhibitor sunitinib, *Lancet*. 370 (2007) 2011–2019. doi:10.1016/S0140-6736(07)61865-0.
- [59] A.K. Abdel-Aziz, A.B. Abdel-Naim, S. Shouman, S. Minucci, M. Elgendy, From resistance to sensitivity: Insights and implications of biphasic modulation of autophagy by sunitinib, *Front. Pharmacol.* 8 (2017) 718. doi:10.3389/fphar.2017.00718.
- [60] A.K. Abdel-Aziz, I. Pallavicini, E. Ceccacci, G. Meroni, M.K. Saadeldin, M. Varasi, S. Minucci, Tuning mTORC1 activity dictates the response to LSD1 inhibition of acute myeloid leukemia, *Haematologica*. 105 (2020) 2105–2117. doi:10.3324/haematol.2019.224501.
- [61] A.K. Abdel-Aziz, S.S.E. Azab, S.S. Youssef, A.M. El-Sayed, E. El-Demerdash, S. Shouman, Modulation of imatinib cytotoxicity by selenite in HCT116 colorectal cancer cells, *Basic Clin. Pharmacol. Toxicol.* 116 (2015) 37–46. doi:10.1111/bcpt.12281.
- [62] A.K. Abdel-Aziz, S. Shouman, E. El-Demerdash, M. Elgendy, A.B. Abdel-Naim, Chloroquine synergizes sunitinib cytotoxicity via modulating autophagic, apoptotic and angiogenic

machineries, *Chem. Biol. Interact.* 217 (2014) 28–40. doi:10.1016/j.cbi.2014.04.007.